ACS APPLIED MATERIALS & INTERFACES

Research Article

www.acsami.org

# Enzyme-Induced and Tumor-Targeted Drug Delivery System Based on Multifunctional Mesoporous Silica Nanoparticles

Yin-Jia Cheng, Guo-Feng Luo, Jing-Yi Zhu, Xiao-Ding Xu, Xuan Zeng, Dong-Bing Cheng, You-Mei Li, Yan Wu, Xian-Zheng Zhang, Ren-Xi Zhuo, and Feng He*

Key Laboratory of Biomedical Polymers of Ministry of Education, Department of Chemistry, Wuhan University, Wuhan 430072, China

Supporting Information

**ABSTRACT:** Functional mesoporous silica particles have attracted growing research interest for controlled drug delivery in targeted cancer therapy. For the purpose of efficient targeting tumor cells and reducing the adverse effect of antitumor drug doxorubicin (DOX), biocompatible and enzyme-responsive mesoporous silica nanoparticles (MSNs) with tumor specificity were desired. To construct these functional MSNs, the classic rotaxane structure formed between alkoxysilane tether and $\alpha$-cyclodextrin ($\alpha$-CD) was employed to anchor onto the orifices of MSNs as gatekeeper in this work. After subsequent modification by multifunctional peptide (azido-GFLGR$_7$RGDS with tumor-targeting, membrane-penetrating, and cathepsin B-responsive functions) to stabilize the gatekeeper, the resulting functional MSNs showed a strong ability to load and seal DOX in their nanopores. When incubating these DOX-loaded MSNs with tumor and normal cells, the nanoparticles could efficiently employ their surface-encoded RGDS and continuous seven arginine ($R_7$) sequences to target tumor cells, penetrate the cell membrane, and enter tumor cells. Because cathepsin B overexpressed in late endosomes and lysosomes of tumor cells could specifically hydrolyze GFLG sequences of the nanovalves, the DOX-loaded MSNs showed an "off-on" drug release behavior that ~80% loaded DOX could be released within 24 h and thus showed a high rate of apoptosis. Furthermore, in vitro cellular experiments indicated that DOX-loaded MSNs (DOX@MSN-GFLGR$_7$RGDS/$\alpha$-CD) had high growth inhibition toward $\alpha_v\beta_3$-positive HeLa cancerous cells. The research might offer a practical way for designing the tumor-targeted and enzyme-induced drug delivery system for cancer therapy.

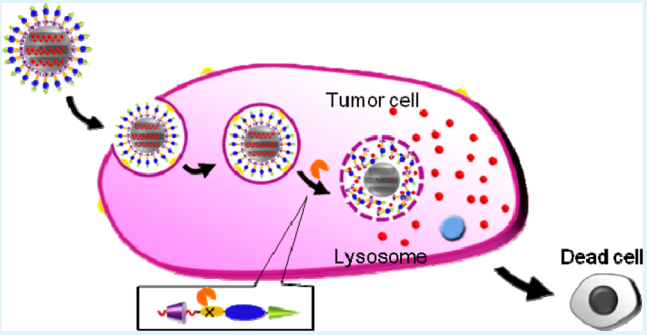


**KEYWORDS:** *mesoporous silica nanoparticle, rotaxane, peptide, enzyme-sensitive, targeted drug delivery*

## 1. INTRODUCTION

Cancer is one of the most terrible causes of death worldwide, and incidences of cancer continue to increase in recent years. Currently, conventional chemotherapy is still applied for cancer therapy.[1] However, there are many barriers that hinder their clinical translation, including unsatisfied drug loading, lack of active targeting to tumor cells, and undesirable drug leakage during sample storage or blood circulation. To address aforementioned issues, the rational design of tumor-specific stimuli-responsive drug delivery carriers to enhance therapeutic efficiency and reduce side effects to healthy organs are of the utmost importance.[2,3] Among various kinds of nanocarriers, mesoporous silica nanoparticles (MSNs) with porous reservoirs, MCM-41 in particular, have been widely used in recent years as solid support for drug storage and delivery due to their advantageous properties, such as chemically inert, easy functionalization, low toxicity, and large loading capacity.[4−6] To be an excellent nanodrug delivery system (nano-DDS), functionalized MSNs are usually constructed by covering the surface of MSNs with nanovalves including rotaxanes,[7−9] polypseudorotaxanes,[10] cucurbiturils,[11] magnetic nanoparticles,[12,13] gold nanoparticles,[14,15] dendrimers,[16] antibodies,[17] and anions.[18] These systems have been designed toward the aim of retaining drugs in the pore until gatekeepers were removed by external stimuli such as pH, temperature, redox potential, light, and enzyme.[19−23] Among those various gatekeepers, cyclodextrin (CD)-based molecular machines in various forms can effectively block the pore of MSNs through cleavable intermediate linkages and dissociate to achieve a rapid drug release in response to various external stimuli.[24−27] Recently, enzyme-sensitive drug delivery has been utilized as a very interesting approach, due to the mild reaction conditions, high specificity, and low level of damage to body tissues. More importantly, many types of enzymes show a high level of expression in tumor tissues and cancer cells but no or relatively low level of expression in healthy tissues or normal cells. For example, cathepsin B, which can specifically hydrolyze Gly-Phe-Leu-Gly (GFLG) sequence, is a late endosomal and lysosomal

Received: January 25, 2015
Accepted: April 20, 2015
Published: April 20, 2015





DOI: 10.1021/acsami.5b00752
ACS Appl. Mater. Interfaces 2015, 7, 9078−9087

protease overexpressed in various types of tumors.[23,28−30] In addition, targeted drug delivery is another attractive way for cancer therapy. Active targeting drug delivery promotes a high drug concentration in the targeted lesion site, achieving more effective tumor suppression and reducing the associated toxicity to normal cells. It is well-known that many moieties, such as peptides, folic acid, glycyrrhetinic acid, or antibodies, can be used as targeting ligands.[19,20,22,31,32] Arg-Gly-Asp-Ser (RGDS), for instance, has been reported to have specific recognition of $\alpha_v\beta_3$-integrin receptor overexpressed cell types such as endothelial cells, platelets, macrophages, and melanomas.[19,22] Moreover, the design of capped MSNs that combine properties of multifunctional peptide and mesoporous nanoparticles is an appealing approach.

Herein, we designed a drug delivery carrier based on rotaxane-modified MSNs. Multifunctional rotaxanes on MSNs were fabricated by using alkoxysilane tether, $\alpha$-cyclodextrin ($\alpha$-CD), and multifunctional peptides. The conjugated oligopeptides were composed of three functional segments, including a cell-penetrating peptide of seven arginine ($R_7$) sequence, an enzyme-cleavable peptide of GFLG, and a tumor-targeting peptide of RGDS (Scheme 1A). When incubating the DOX-loaded MSNs with tumor and normal cells, the multifunctional nanoparticles could target tumor cells via the specific interaction between RGDS and integrins receptor $\alpha_v\beta_3$ overexpressed on tumor cells, followed by penetrating cell membrane with the aid of $R_7$ sequence. After cellular uptake, drug-loaded MSNs released the encapsulated drug quickly due to the breakage of GFLG peptide cleaved by cathepsin B, resulting in enhanced antitumor activity (Scheme 1B−F). This effective enzyme-responsive drug release system might have great potential in the applications of nanomedicine.

**Scheme 1**[a]

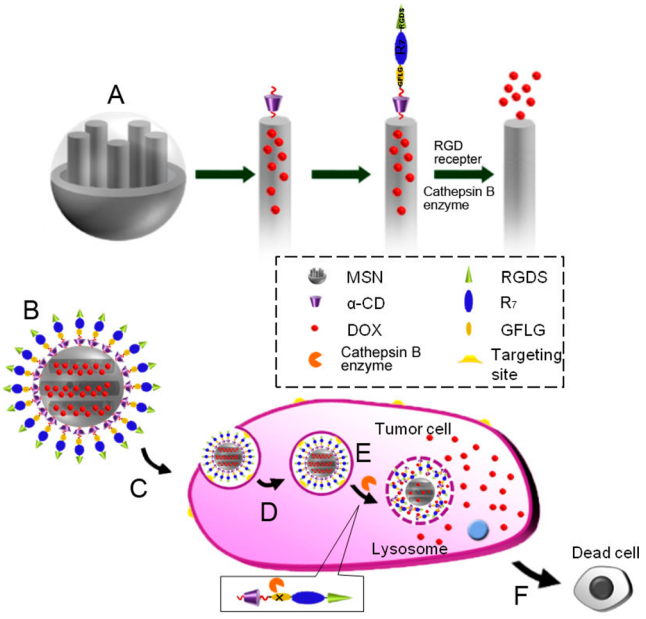


[a](A) Functionalization procedure of the MSNs. (B) Drug-loaded MSNs under physiological condition. (C) RGDS-targeted to the tumor cell. (D) Endocytosis into specific tumor cell. (E) Cathepsin B enzyme-triggered drug release in cytoplasm. (F) Apoptosis of the tumor cell.

## 2. EXPERIMENTAL SECTION

**2.1. Materials.** *N*-Cetyltrimethylammonium bromide (CTAB), sodium hydroxide (NaOH), tetraethylorthosilicate (TEOS), copper(II) sulfate pentahydrate ($CuSO_4{\cdot}5H_2O$), sodium ascorbate (NaAsc), ethylene diamine tetraacetic acid (EDTA), triethylamine (TEA), ninhydrin, phenol, piperidine, dichloromethane (DCM), and trifluoroacetic acid (TFA) were purchased from Shanghai Reagent Chemical Co. and used as received. *N*,*N*-Dimethylformamide (DMF) was purchased from Shanghai Reagent Chemical Co. and distilled prior to use. 2-Chlorotrityl chloride resin (1.21 mmol/g), *N*-fluorenyl-9-methoxycarbonyl (FMOC)-protected L-amino acids (Fmoc-Phe-OH, Fmoc-Gly-OH, Fmoc-Arg(Pbf)−OH, Fmoc-Asp(OtBu)−OH, Fmoc-Ser(tBu)−OH, Fmoc-Leu-OH), diisopropylethylamine (DiEA), 1,2-ethanedithiol (EDT), triisopropylsilane (TIS), *N*-hydroxybenzotriazole (HOBt), and *o*-benzotriazol-*N*,*N*,*N*′,*N*′-tetramethyluronium hexafluorophosphate (HBTU) were obtained from GL Biochem Ltd. and used as received. Azidoacetic acid was synthesized according to our previous study.[38] Doxorubicin hydrochloride (DOX) was received from Zhejiang Hisun Pharmaceutical Co. (China). Propargyl bromide and $\gamma$-(2-aminoethyl)-aminopropyl trimethoxysilane (AAPTMS) were obtained from Sigma-Aldrich Reagent.

Cervical cancer cells (HeLa) and African green monkey SV40-transformed kidney fibroblast cells (COS7) were purchased from Cell Bank of Chinese Academy of Sciences (Shanghai, China). Dulbecco's Modified Eagle's Medium (DMEM), Dulbecco's phosphate buffered saline (PBS), fetal bovine serum (FBS), penicillin-streptomycin, and 3-(4,5-dimethylthiazol-2-yl)-2,5-diphenyltetrazolium bromide (MTT) were acquired from Invitrogen. All other solvents and reagents were of analytical grade and used as received.

**2.2. Synthesis of Azido-GFLGR$_7$RGDS and Arg-Gly-Asp-Ser.** All peptides applied in this work were synthesized on the 2-chlorotrityl chloride resin (1.21 mmol/g) manually via a standard Fmoc-based solid phase peptide synthesis (SPPS).[33] The resin was washed with DCM (three times) and DMF (three times) and then allowed to swell in DMF for 30 min. After draining the DMF solution out, a DMF solution of the mixture of Fmoc-protected amino acid (0.6 equiv relative to resin loading) and DiEA (3 equiv) was added to the resin and shaken for 30 min at room temperature. After the reaction solution was removed and washed with DMF (three times), a DMF solution of the mixture of methanol (8 equiv) and DiEA (10 equiv) was added to react with the active chloride on the resin for 30 min. Subsequently, 25% piperidine/DMF (v/v) solution was added to remove the Fmoc-protected groups. After it was shaken for 20 min at room temperature, the reaction solution was drained off, and the resin was washed with DMF (three times). The presence of free amino groups was indicated by a blue color in the Kaiser test. Thereafter, a DMF solution of the mixture of Fmoc protected amino acid (4 equiv), HBTU (4 equiv), HOBt (4 equiv) and DiEA (6 equiv) was added. After shaking for 1.5 h at room temperature, the reaction solution was drained off and the resin was washed with DMF (three times). The absence of free amino groups was indicated by a yellow color in the Kaiser test. After repetition of the deprotection and acylation reaction to obtain the required amino acid sequence, the resin was finally washed with DMF (three times) and DCM (three times). Cleavage of the expected peptide and the removal of the protected groups were performed using a mixture of TFA, TIS, distilled water, phenol, and EDT in the ratio of 82.5:4.5:4.5:6:2.5. After it was shaken at room temperature for 2 h, the cleavage mixture and three subsequent TFA washings were collected. The combined solution was concentrated, and cold ether was then added to precipitate the product. After it was washed with cold ether (five times), the precipitate was collected and dried under vacuum. MALDI-TOF-MS of azido-GFLGR$_7$RGDS, 1985.7 $[M + H]^+$ (Supporting Information, Figure S1). ESI-MS of RGDS, 434.2 $[M + H]^+$ (Supporting Information, Figure S2).

**2.3. Synthesis of Mesoporous Silica Nanoparticles.** MCM-41-type MSNs were synthesized according to the previous literature.[34] Briefly, CTAB (1.0 g, 2.74 mmol) was first dissolved in 480 mL of NaOH aqueous solution (0.01 M). The solution was stirred at 80 °C for 15 min. Subsequently, TEOS (5.0 g, 22.4 mmol) was added, and


DOI: 10.1021/acsami.5b00752
ACS Appl. Mater. Interfaces 2015, 7, 9078−9087

the mixture was allowed to stir for another 2 h. To collect the formed MSNs, the nanoparticle solution was centrifuged at 8500 rpm for 10 min and then washed with DI water (four times) and methanol (four times), followed by vacuum drying. The extraction of residual CTAB was performed by suspending the MSNs in a mixture of methanol and HCl (16:1 v/v). After they were stirred at 60 °C for 48 h, the purified MSNs were collected by centrifuging the nanoparticle solution (8500 rpm, 10 min), washing with methanol (four times) and obtained after vacuum drying.

**2.4. Synthesis of Mesoporous Silica Nanoparticle-$NH_2$.** MSNs (1.0 g) were suspended in 80 mL of MeOH by ultrasonic dispersion. Then 6 mL of γ-(2-aminoethyl)-aminopropyl trimethoxysilane was added for reacting 24 h at room temperature. The resulting nanoparticles were obtained by centrifugation (8500 rpm, 10 min) and washed with methanol several times before vacuum drying. The extraction of CTAB resided in the nanoparticles was carried out in a mixture of methanol and HCl (16:1 v/v) for 48 h at 60 °C. MSN-$NH_2$ nanoparticles were obtained after centrifugation (8500 rpm, 10 min), washing with methanol (four times) and vacuum drying.

**2.5. Synthesis of Mesoporous Silica Nanoparticle-Alkyne.** MSN-$NH_2$ (500 mg) nanoparticles were suspended in 20 mL of MeOH by ultrasonic dispersion. Propargyl bromide (4 mL, 51.1 mmol) was added and reacted for 24 h at room temperature. The nanoparticles were obtained by centrifugation (8500 rpm, 10 min), washed with methanol several times, and finally dried under high vacuum to obtain MSN-alkyne.

**2.6. Synthesis of MSN-GFLGR$_7$RGDS/α-CD.** For preparation of the solid MSN-GFLGR$_7$RGDS/α-CD, 100 mg MSN-alkyne nanoparticles were dispersed in 20 mL of DI water, 200 mg of α-CD was introduced, and the mixture was stirred at 5 °C for 24 h. Then, azido-GFLGR$_7$RGDS (100 mg, 0.05 mmol), NaAsc (198.1 mg, 1.0 mmol), and $CuSO_4{\cdot}5H_2O$ (125 mg, 0.5 mmol) were added to above reaction mixture and stirred for 3 d at room temperature under $N_2$ protection. The expected MSN-GFLGR$_7$RGDS/α-CD nanoparticles were collected by centrifugation at 8500 rpm for 10 min, followed by washing with methanol (four times) to remove the unreacted and adsorbed molecules, followed by vacuum drying.

**2.7. Loading of Drug and Sealing in Cargo with Azido-GFLGR$_7$RGDS.** MSN-alkyne nanoparticles (0.1 g) and DOX·HCl (10 mg) were dispersed in 10 mL of PBS buffer (10 mM, pH 7.4). At room temperature, the mixture was stirred in dark for 24 h, and DOX·HCl was thus loaded into the mesopores by free diffusion. Subsequently, a solution of α-CD (0.05 g/mL) was added, and the mixture was stirred at 5 °C for 24 h to allow the threading of α-CD ring onto the alkyl chain of DOX@MSN-alkyne. Then, azido-GFLGR$_7$RGDS (0.1 g, 0.05 mmol), $CuSO_4{\cdot}5H_2O$ (0.13 g, 0.5 mmol), and NaAsc (0.2 g, 1.0 mmol) were added, and the mixture was stirred under nitrogen atmosphere for 3 d. Through the click reaction between azido and alkyne functional groups, the azido-GFLGR$_7$RGDS was conjugated to the surface of DOX@MSN-alkyne/α-CD to prevent the removal of α-CD ring. The resulting nanoparticles (DOX@MSN-GFLGR$_7$RGDS/α-CD) were collected by centrifugation at 8500 rpm for 10 min, followed by washing with methanol (four times) and vacuum drying.

To determine the drug-loading content (DLC) and drug-loading efficiency (DLE), DOX@MSN-GFLGR$_7$RGDS/α-CD nanoparticles (0.1 mg) were dissolved in 0.1 M HF solution, since HF solution is highly corrosive and can destroy mesoporous silica structure completely.[21] Then the dissolution was adjusted to pH ≈ 7.4 by NaOH solution and studied by fluorescence analysis for DOX concentration. The amount of DOX was measured by an RF-530/PC spectrofluorophotometer (Shimadzu) with $\lambda_{ex}$ = 480 nm and $\lambda_{em}$ = 555 nm (DOX) and analyzed with a standard calibration curve experimentally obtained. The DLC and DLE values of DOX@MSN-GFLGR$_7$RGDS/α-CD were calculated as follows: DLC (wt %) = (weight of loaded drug/weight of drug-loaded MSNs) × 100%. DLE (wt %) = (mass of loaded drug/mass of feed drug) × 100%.

**2.8. In Vitro Enzyme-Induced Drug Release.** The enzyme-responsive drug-release experiments were performed in PBS (10 mM, pH 7.4, and pH 5.0) in triplicate for each sample, and DOX-loaded nanoparticles (3 mg) were incubated in 3 mL of PBS (10 mM, pH 7.4, and pH 5.0) with or without 20 U cathepsin B for comparison. The sample solution (1 mg/mL) was transferred to a dialysis bag (MWCO 12000 Da) and immersed in 10 mL of PBS shaken in a water bath at 37 °C. At predetermined time intervals, 3 mL of released solution was replaced by 3 mL of fresh media for each sample. The performance of DOX release was monitored by using an RF-530/PC spectrofluorophotometer (Shimadzu) with $\lambda_{ex}$ = 480 nm and $\lambda_{em}$ = 555 nm (DOX); the average value of three independent experiments was collected, and the cumulative DOX release was calculated as follows:

$$\text{cumulative DOX release}(\%) = (M_t/M_\infty) \times 100$$

where $M_t$ is the amount of DOX released from the MSNs and $M_\infty$ is the amount of DOX loaded in the MSNs.

**2.9. Western Blot Analysis of Cathepsin B Protein Expression.** HeLa cells and COS7 cells were planted in 24-well plates at a density of $5 \times 10^4$ cells/well and incubated in 1 mL of DMEM for 24 h under a humidified 5% $CO_2$ atmosphere. Subsequently, cells were thoroughly washed with PBS buffer, harvested by scraping, and lysed twice in an equal volume of lysosomal buffer (250 mM sucrose, 20 mM HEPES, pH 7.2). The protein concentration of lysosomal extracts was determined by using the Bicinchoninic Acid (BCA) assay. Thereafter, the lysosomal extracts were separated on a 10% SDS-PAGE (polyacrylamide gelelectrophoresis, 15 μL per lane) for electrophoresis assay. The proteins were then transferred from SDS gel surface to a 0.45 μm PVDF membrane (Millipore) by using semi-dry transfer cell (Biorad). Subsequently, the membranes were blocked with 5% skim milk in Tris-buffered saline-Tween 20 (TBST) for 1 h, followed by incubating with anticathepsin B at room temperature for 1 h. After washing with TBST (three times), the membranes were incubated with a horseradish peroxidase-conjugated Affini Pure Goat Anti-Rabbit IgG (1:10 000 dilution) in TBST for 30 min. After it was washed with TBST (three times), the cathepsin B protein was detected on an enhanced chemiluminescence (ECL; Pierce), and the expressions were quantified by using Alpha software (Molecular Dynamics, Sunnyvale, CA). The expression of glyceraldehyde-3-phosphate dehydrogenase (GAPDH) protein was also detected as control.

**2.10. Intracellular Uptake.** HeLa and COS7 cells were separately seeded in a six-well plate and cultured in 1 mL of DMEM containing 10% FBS for 24 h under a humidified 5% $CO_2$ atmosphere. Subsequently, DOX@MSN-GFLGR$_7$RGDS/α-CD nanoparticles dispersed in DMEM (0.1 mg/mL) was added to each well. After 4 h of incubation, the nuclei were stained by blue molecular probe (Hoechst 33258) for 15 min. After the medium was removed and subsequently washed with PBS buffer, the cells were viewed under a confocal laser scanning microscope (CLSM, Nikon C1-si TE2000, Japan) with the excitation at 408 nm for blue molecular probe and 488 nm for DOX.

**2.11. Flow Cytometry.** HeLa and COS 7 cells were seeded in a six-well dish and cultured in the DMEM containing 10% FBS for 24 h under a humidified 5% $CO_2$ atmosphere, respectively. Then, DMEM containing DOX@MSN-GFLGR$_7$RGDS/α-CD (DOX: 5 μg/mL) was added in each well and incubated for another 4 h. Then, the medium (DMEM containing 10% FBS) was removed and cleaned with PBS three times. The cells were digested by trypsin and harvested by centrifugation (10 000 rpm for 5 min), and then studied on a flow cytometer (BD FACSAria TM III, USA). The DMEM without the treatment of DOX-loaded nanoparticles was used as a blank control to identify living cells. Furthermore, the cellular uptake of DOX@MSN-GFLGR$_7$RDGS/α-CD in the presence of free RGDS peptide was also studied by flow cytometry.

**2.12. In Vitro Cytotoxicity Assay.** HeLa and COS7 cells were separately seeded in a 96-well plate and cultured in 100 μL of DMEM containing 10% FBS for 24 h under a humidified 5% $CO_2$ atm. Subsequently, DOX@MSN-GFLGR$_7$RGDS/α-CD nanoparticles dispersed in DMEM were added to each well, and the cells were incubated for another 48 h. After the medium was replaced with fresh DMEM, MTT (20 μL, 5 mg/mL in PBS) solution was added to each well. After 4 h of incubation, the medium was removed, and 150 μL of DMSO was added. After the solution was shaken at room temperature


DOI: 10.1021/acsami.5b00752
ACS Appl. Mater. Interfaces 2015, 7, 9078−9087

**Scheme 2. Preparation of MSN-GFLGR$_7$RGDS/$\alpha$-CD**

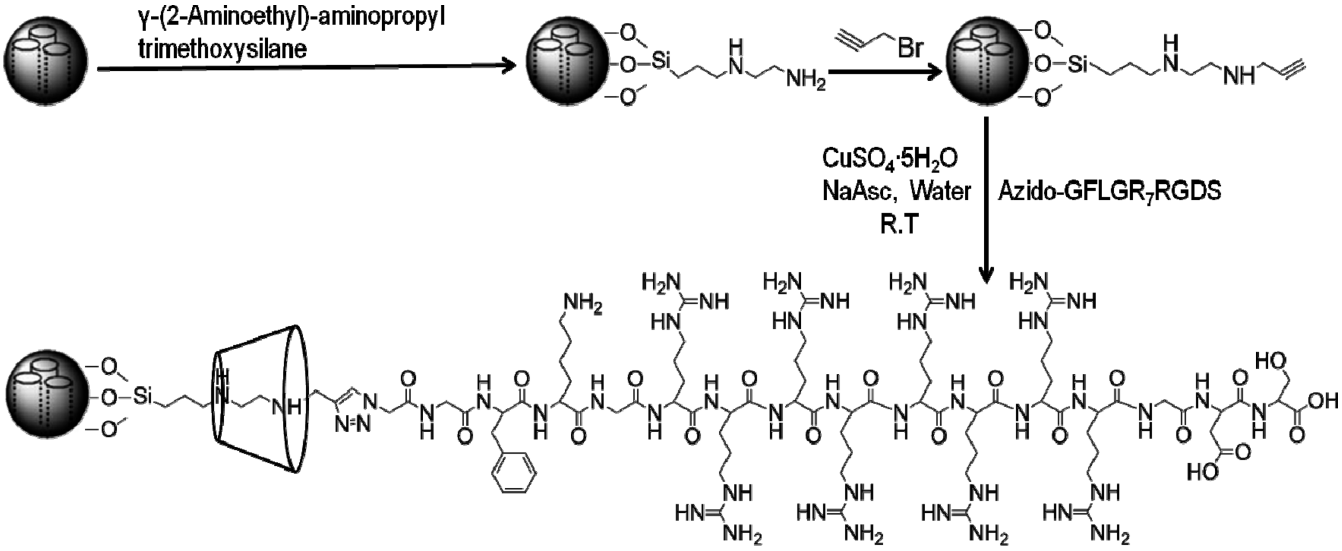


for several minutes, the optical density (OD) was measured at 570 nm with a microplate reader model 550 (BIO-RAD, USA). The average value of four independent experiments was collected, and the cell viability was calculated as follows:

$$\text{cell viability}(\%) = (\text{OD}_{\text{sample}}/\text{OD}_{\text{control}}) \times 100$$

where $\text{OD}_{\text{control}}$ is obtained in the absence of DOX@MSN-GFLGR$_7$RGDS/$\alpha$-CD nanoparticles, and $\text{OD}_{\text{sample}}$ is obtained in the presence of DOX@MSN-GFLGR$_7$RGDS/$\alpha$-CD nanoparticles.

## 3. RESULTS AND DISCUSSION

**3.1. Preparation and Characterization of Blank MSNs and DOX@MSN-GFLGR$_7$RGDS/$\alpha$-CD.** Scheme 1 illustrated the rational design of enzyme-responsive DOX@MSN-GFLGR$_7$RDGS/$\alpha$-CD nanoparticles for RGDS-targeted and enzyme-induced release of anticancer drug DOX in living cells. DOX@MSN-GFLGR$_7$RDGS/$\alpha$-CD could reach the specific tumor sites and internalize into tumor cells quickly. When incubated with tumor cells, the release of anticancer drug would be triggered since $\alpha$-CD gatekeeper could be removed due to the enzymatic hydrolysis of GFLG linker by lysosomal enzyme inside the tumor cells. Detailed grafting procedure of MSN-GFLGR$_7$RGDS/$\alpha$-CD was described in Scheme 2, MCM-41-type MSNs were synthesized and functionalized with amine groups by reacting with AAPTMS, and the surfactant templating agent CTAB was extracted to give the hexagonally arranged mesopores. MSN-$NH_2$ was further reacted with propargyl bromide to obtain MSN-alkyne. After the drug was loaded, a solution of $\alpha$-CD was added to cap the tether, and then the peptide stopper (azido-GFLGR$_7$RGDS) was coupled at the terminus of tether via copper(II)-catalyzed Huisgen azide/alkyne cycloaddition "click" reaction, resulting in the formation of rotaxane structure.

The morphology of the blank MSNs were observed by TEM. As presented in Figure 1A, the MSN showed a uniform and well-defined two-dimensional hexagonal mesostructure (Figure 1C) with an average diameter of ~130 nm, which was smaller than the result of DLS analysis (~235.6 nm, PDI 0.13, Supporting Information, Figure S3). This difference was mainly attributed to the different sample states, that is, the dry state in TEM observation but wet state in DLS analysis.[35] The mesostructure of the MSN was further proven by nitrogen

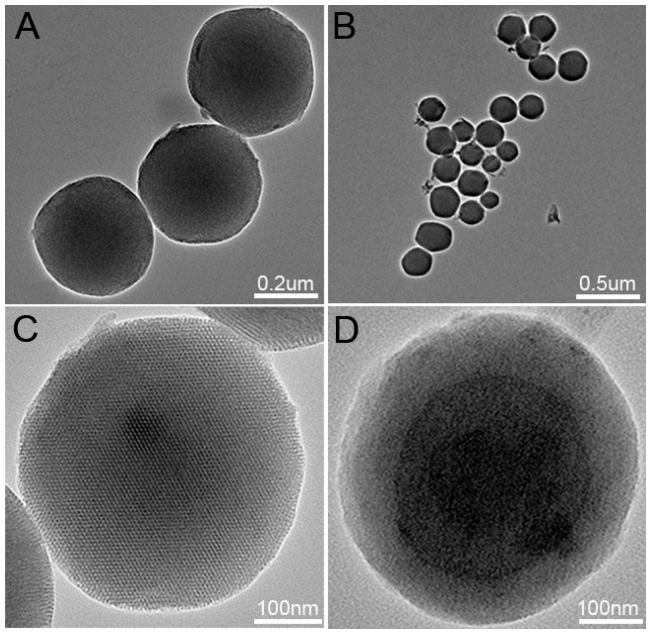


**Figure 1.** TEM images of blank MSNs (A, C) and DOX@MSN-GFLGR$_7$RGDS/$\alpha$-CD (B, D) nanoparticles.

adsorption/desorption isotherm (Figure 2A). The MSNs have well-defined mesoporous nanopores with an average diameter of ~3.86 nm (Figure 2B) and high surface areas of 1136.74 $m^2$/g (Supporting Information, Table S1). After cargo loading and $\alpha$-CD capping, there was an obvious decrease in the pore volume and pore diameter of particles (Figure 2B), indicating that the nanopores were successfully plugged up by the incorporated $\alpha$-CD rings. Besides nitrogen adsorption/desorption isotherm, zeta potential and FT-IR analyses were also employed to monitor the modification of the MSNs. From the zeta potential summarized in Table 1, the blank MSNs were negatively charged with a zeta potential of −24.76 mV, which jumped to +21.04 mV after amine modification. After reaction with propargyl bromide, the zeta potential decreased to +5.23 mV since most of the ionized amine groups had changed into un-ionized amide groups. Further conjugation with azido-GFLGR$_7$RGDS, which is rich in positively charged arginine


DOI: 10.1021/acsami.5b00752
ACS Appl. Mater. Interfaces 2015, 7, 9078−9087

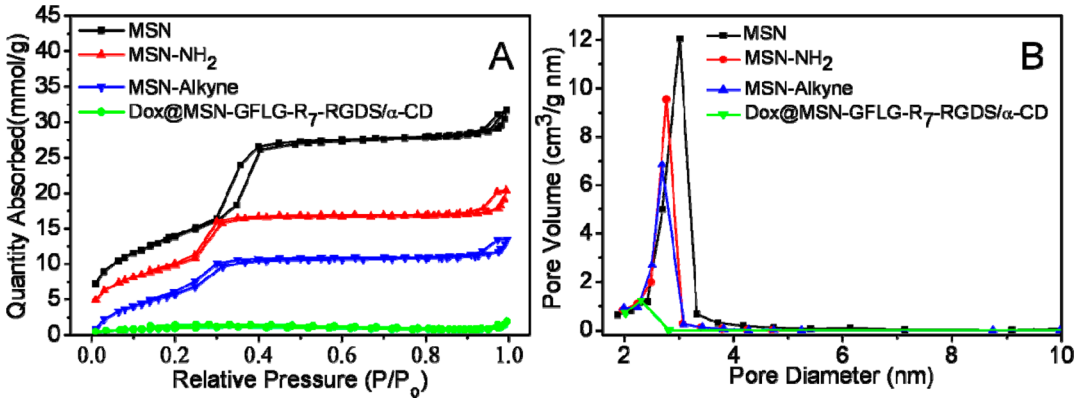


**Figure 2.** BET nitrogen adsorption/desorption isotherms (A) and BJH pore size distribution (B) of different nanoparticles.

**Table 1. Zeta Potential of Different Nanoparticles in PBS (pH 7.4, 10 mM) at 37 °C**

| sample | zeta potential (mV) |
|---|---|
| MSN | −24.76 |
| MSN-$NH_2$ | 21.04 |
| MSN-alkyne | 5.23 |
| MSN-GFLGR$_7$RGDS/α-CD | 32.57 |
| DOX@MSN-GFLGR$_7$RGDS/α-CD | 28.14 |

residues, zeta potential of the formed MSN-GFLGR$_7$RGDS/α-CD nanoparticles dramatically increased to +32.57 mV. The result of FT-IR analysis (Supporting Information, Figure S4) was consistent with that of zeta potential change. No signal at 3000−2800 $cm^{-1}$ corresponding to the C−H absorbance of the template agent CTAB indicated the good purity of the blank MSNs. The typical signal at ∼2125 $cm^{-1}$ belonging to the absorbance of alkyne group strongly demonstrated the success in the alkyne modification. Because of the click reaction between alkyne and azido groups, the absorbance at ∼2125 $cm^{-1}$ disappeared after the formation of DOX@MSN-GFLGR$_7$RGDS/α-CD nanoparticles.

To exactly determine the amount of each component in the DOX@MSN-GFLGR$_7$RGDS/α-CD nanoparticles, TGA analysis was used to examine the weight loss of the MSNs after each modification. From the TGA curves (Figure 3), when the temperature rose to 800 °C, the weight loss of blank MSNs and DOX@MSN-GFLGR$_7$RGDS/α-CD nanoparticles were ∼10.2% and 29.8%, respectively. From the weight loss in Figure 3, the mass of grafted amino groups, α-CD rings and

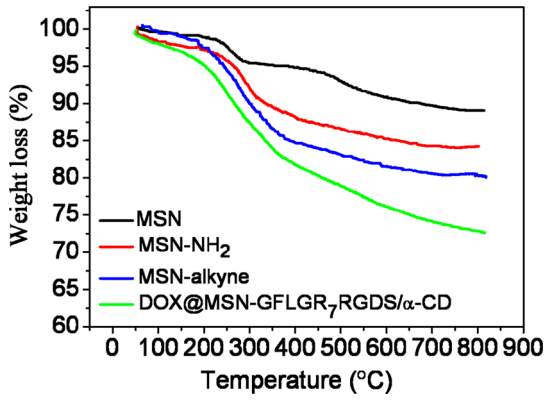


**Figure 3.** TGA curves of the functional MSNs.

multifunctional peptide molecules in MSN-GFLGR$_7$RGDS/α-CD could be, respectively, calculated as 853.2, 330.1, and 252.6 mmol/kg $SiO_2$ according to the following equation:

$$\frac{\frac{W_1}{100 - W_1} \times 100 - W_2}{M \times 100}$$

where $W_1$ represents the weight loss relative to the functionalized MSNs, $W_2$ is the weight loss of MSNs before modification, and $M$ is the molecular weight of relative grafted material.

**3.2. Enzyme-Induced Drug Release.** The in vitro release behaviors were investigated in PBS buffer at a pH of 7.4 (physiological environment) and 5.0 (lysosome environment). Herein, the DLC and DLE values of DOX@MSN-GFLGR7RGDS/α-CD nanoparticles were ∼4.3% and 35.7%, respectively. The detailed drug-release profile of DOX@MSN-GFLGR7RGDS/α-CD nanoparticles is shown in Figure 4. In

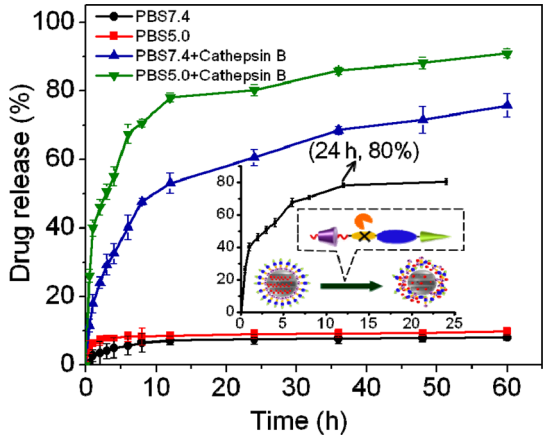


**Figure 4.** In vitro drug release behavior of DOX@MSN-GFLGR$_7$RGDS/α-CD in PBS buffer (pH 7.4 and 5.0) at physiological temperature (37 °C). The concentration of cathepsin B added in PBS was 20 U.

the presence of cathepsin B, ∼60% loaded DOX has been released from the DOX@MSN-GFLGR$_7$RGDS/α-CD nanoparticles incubated in pH 7.4 PBS buffer for 24 h. In contrast, in the absence of cathepsin B (20 U), due to the protection of the gatekeeper on the surface of the MSNs, less than 10% loaded DOX was released within the same time scale. This result indicated that the cathepsin B could cleave the GFLG sequence and thus induce the removal of the gatekeeper from the surface


DOI: 10.1021/acsami.5b00752
ACS Appl. Mater. Interfaces 2015, 7, 9078−9087

of the MSNs, which was further proved by the DOX release behavior in pH 5.0 PBS buffer. Because of the relatively high activity of cathepsin B under acidic environment,[29] the addition of cathepsin B led to a much faster DOX release rate at pH 5.0 than that at pH 7.4, and ~80% loaded DOX has been released from the DOX@MSN-GFLGR$_7$RGDS/$\alpha$-CD nanoparticles. Since there was no cathepsin B to remove gatekeeper, the drug release rate is extremely slow even incubating the DOX@MSN-GFLGR$_7$RGDS/$\alpha$-CD nanoparticles in pH 5.0 PBS buffer. It has been demonstrated that the expression of cathepsin B in the endosomes and lysosomes of tumor cells is higher than that of normal cells, and the endo/lysosomes microenvironment is weakly acidic (pH 5−6).[36,37] The relatively fast DOX release rate at pH 5.0 upon the addition of cathepsin B implied that the DOX@MSN-GFLGR$_7$RGDS/$\alpha$-CD nanoparticles could achieve expected off-on release behavior in tumor cells and thus presented a potential application as smart carriers for antitumor drug delivery.

**3.3. Cellular Uptake and Intracellular Drug Release.** After the demonstration of the cathepsin B responsive drug release behavior, the tumor cell line of HeLa and normal cell line of COS7 were chosen to evaluate the targeting and intracellular drug release ability of DOX@MSN-GFLGR$_7$RGDS/$\alpha$-CD nanoparticles. We first employed Western blot to examine the expression of cathepsin B in these two cell lines. As shown in Figure 5, HeLa cells showed a much

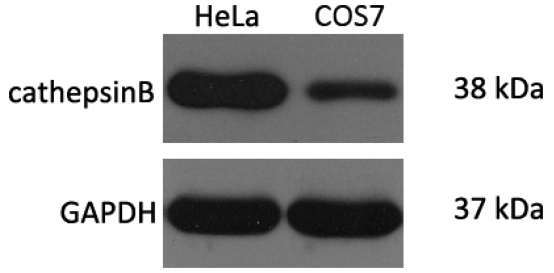


**Figure 5.** Expression of cathepsin B in HeLa and COS 7 cells determined by Western blot.

higher expression of cathepsin B than that of COS7 cells, which was consistent with previous reports that cathepsin B was generally overexpressed in the late endosomes and lysosomes of many types of tumors.[24−26] The detailed cellular uptake of the DOX@MSN-GFLGR$_7$RGDS/$\alpha$-CD nanoparticles was exhibited in Figure 6. Both COS7 (Figure 6A$_2$) and HeLa cells (Figure 6B$_2$) could internalize the DOX@MSN-GFLGR$_7$RGDS/$\alpha$-CD nanoparticles, corresponding to the red fluorescence. In comparison, because of the high expression of integrins $\alpha_v\beta_3$ and $\alpha_v\beta_5$ on HeLa cells,[19,22] the specific recognition between integrins and RGDS sequences on the surface of MSNs led to a higher uptake of the DOX@MSN-GFLGR$_7$RGDS/$\alpha$-CD nanoparticles than that of COS7 cells. The RGDS-mediated targeted uptake of HeLa cells was further proven by the CLSM image in Figure 6C. When HeLa cells were incubated with the mixture of free RGDS (2 $\mu$M) and DOX@MSN-GFLGR$_7$RGDS/$\alpha$-CD nanoparticles, because of competition between free RGDS and the RGDS sequences on the surface of MSNs with integrins, the uptake of DOX@MSN-GFLGR$_7$RGDS/$\alpha$-CD nanoparticles by HeLa cells was extremely low, corresponding to the weak red fluorescence in Figure 6C$_2$. We also evaluated the cellular uptake of free DOX. Because of the absence of selectivity, although COS7 (Figure 6D$_2$) and HeLa (Figure 6E$_2$) cells showed a high uptake of free DOX, there was no significant difference between these two cell lines. The uptake of free DOX was mainly built on the concentration gradient diffusion, and thus the internalized free DOX molecules were distributed in the whole cytoskeleton.[39−42] However, in the case of DOX@MSN-GFLGR$_7$RGDS/$\alpha$-CD, DOX was released from DOX-loaded MSNs in a slow and sustained manner because drug release was only accelerated after cleavage of GFLG triggered by CatB in lysosome. Moreover, since the rate of concentration gradient diffusion was much faster than that of endocytosis, the intensity of red fluorescence in the HeLa cells incubated with free DOX (Figure 6E$_2$) was higher than that incubated with the DOX@MSN-GFLGR$_7$RGDS/$\alpha$-CD nanoparticles (Figure 6B$_2$).

The cellular uptake of the DOX@MSN-GFLGR$_7$RGDS/$\alpha$-CD nanoparticles was quantitatively monitored by flow cytometry. As shown in Figure 6F, with the aid of RGDS-mediated uptake, the intracellular fluorescence of HeLa cells was much stronger than that of COS7 cells. The corresponding mean fluorescence intensity (MFI) of HeLa cells (~6513) was more than 4-fold higher than that of COS7 cells (~1374). For the HeLa cells incubated with the mixture of free RGDS (2 $\mu$M) and the DOX@MSN-GFLGR$_7$RGDS/$\alpha$-CD nanoparticles, due to the competition between free RGDS and the RGDS sequences on the surface of MSNs, the intracellular fluorescence was very weak and the corresponding MFI was around 5-fold weaker than that of HeLa cells only incubated with the DOX@MSN-GFLGR$_7$RGDS/$\alpha$-CD nanoparticles. All these results strongly demonstrated that the DOX@MSN-GFLGR$_7$RGDS/$\alpha$-CD nanoparticles could efficiently use their surface RGDS sequences to target tumor cells, which provides a valuable opportunity to use this nanoplatform for targeted cancer therapy.

**3.4. In Vitro Anticancer Effect.** The in vitro cytotoxicity of drug-free and drug-loaded MSNs was investigated by MTT assay (Figure 7). Figure 7A studied the cell viability of COS7 cells and HeLa cells incubated with blank MSN-GFLGR$_7$RGDS/$\alpha$-CD. In a wide range from 0 to 100 mg/L, drug-free MSNs displayed low cytotoxicity in both cell lines, confirming the good biocompatibility of MSNs. Furthermore, Figure 7B presented the toxicity of DOX@MSN-GFLGR$_7$RGDS/$\alpha$-CD nanoparticles in COS7 and HeLa cells. Because of the high cellular uptake demonstrated in Figure 6B$_2$, DOX@MSN-GFLGR$_7$RGDS/$\alpha$-CD nanoparticles showed a high toxicity in HeLa cells, and less than 20% of the cells were alive at a relative DOX concentration of 5 $\mu$g/mL. In contrast, owing to the absence of RGDS-mediated uptake, the DOX@MSN-GFLGR$_7$RGDS/$\alpha$-CD nanoparticles show a relatively lower toxicity in COS7 cells, and more than 40% of cells were still alive at the same DOX concentration. Similarly, since the competition between free RGDS and the RGDS sequences on the surface of MSNs inhibited the cellular uptake, DOX@MSN-GFLGR$_7$RGDS/$\alpha$-CD nanoparticles showed a lower toxicity in HeLa cells. Although free DOX showed much higher cytotoxicity in both COS7 and HeLa cells than that of the DOX@MSN-GFLGR$_7$RGDS/$\alpha$-CD nanoparticles, there was no selectivity. The half-inhibitory concentration ($IC_{50}$) of the DOX@MSN-GFLGR$_7$RGDS/$\alpha$-CD nanoparticles was summarized in Table 2. The $IC_{50}$ of the DOX@MSN-GFLGR$_7$RGDS/$\alpha$-CD nanoparticles in HeLa cells was ~1.2 $\mu$g/mL, which was more than threefold lower than that in COS7 cells (~3.8 $\mu$g/mL). The competition between free RGDS and the RGDS sequences on the surface of MSNs led to


DOI: 10.1021/acsami.5b00752
ACS Appl. Mater. Interfaces 2015, 7, 9078−9087

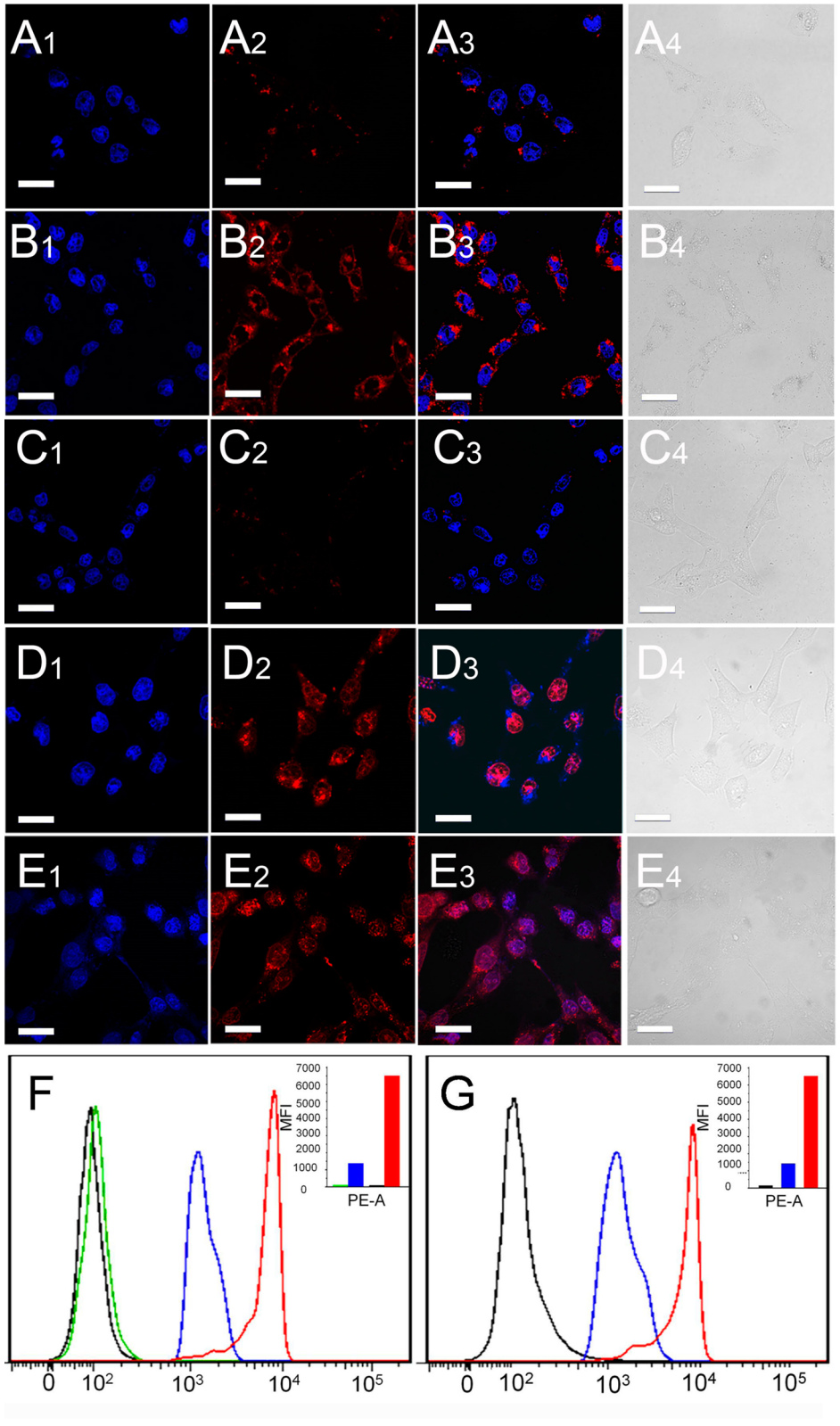


**Figure 6.** (A, B) CLSM images of COS 7 (A) and HeLa (B) cells incubated with the DOX@MSN-GFLGR$_7$RGDS/$\alpha$-CD nanoparticles (relative DOX concentration, 5 $\mu$g/mL) for 4 h. (C) CLSM images of HeLa cells incubated with the mixture of free RGDS (2 $\mu$M) and the DOX@MSN-GFLGR$_7$RGDS/$\alpha$-CD nanoparticles (relative DOX concentration, 5 $\mu$g/mL) for 4 h. (D, E) CLSM images of COS 7 (D) and HeLa (E) cells incubated with free DOX (5 $\mu$g/mL) for 4 h. ($A_1$, $A_2$, $B_1$, $B_2$, $C_1$, $C_2$, $D_1$, $D_2$, $E_1$, $E_2$) confocal fluorescence images; ($A_3$) confocal fluorescence image overlay of $A_1$ and $A_2$; ($B_3$) confocal fluorescence image overlay of $B_1$ and $B_2$; ($C_3$) confocal fluorescence image overlay of $C_1$ and $C_2$; ($D_3$) confocal fluorescence image overlay of $D_1$ and $D_2$; ($E_3$) confocal fluorescence image overlay of $E_1$ and $E_2$; ($A_4$, $B_4$, $C_4$, $D_4$, $E_4$) bright-field images. (The scale bar is 30 $\mu$m). (F) Flow cytometry analysis and MFI of COS7 and HeLa cells, respectively, incubated with the DOX@MSN-GFLGR$_7$RGDS/$\alpha$-CD nanoparticles for 4 h. (G) Flow cytometry analysis and MFI of HeLa cells incubated with the DOX@MSN-GFLGR$_7$RGDS/$\alpha$-CD nanoparticles in the absence and presence of free RGDS (2 $\mu$M) for 4 h.



DOI: 10.1021/acsami.5b00752
*ACS Appl. Mater. Interfaces* 2015, 7, 9078−9087

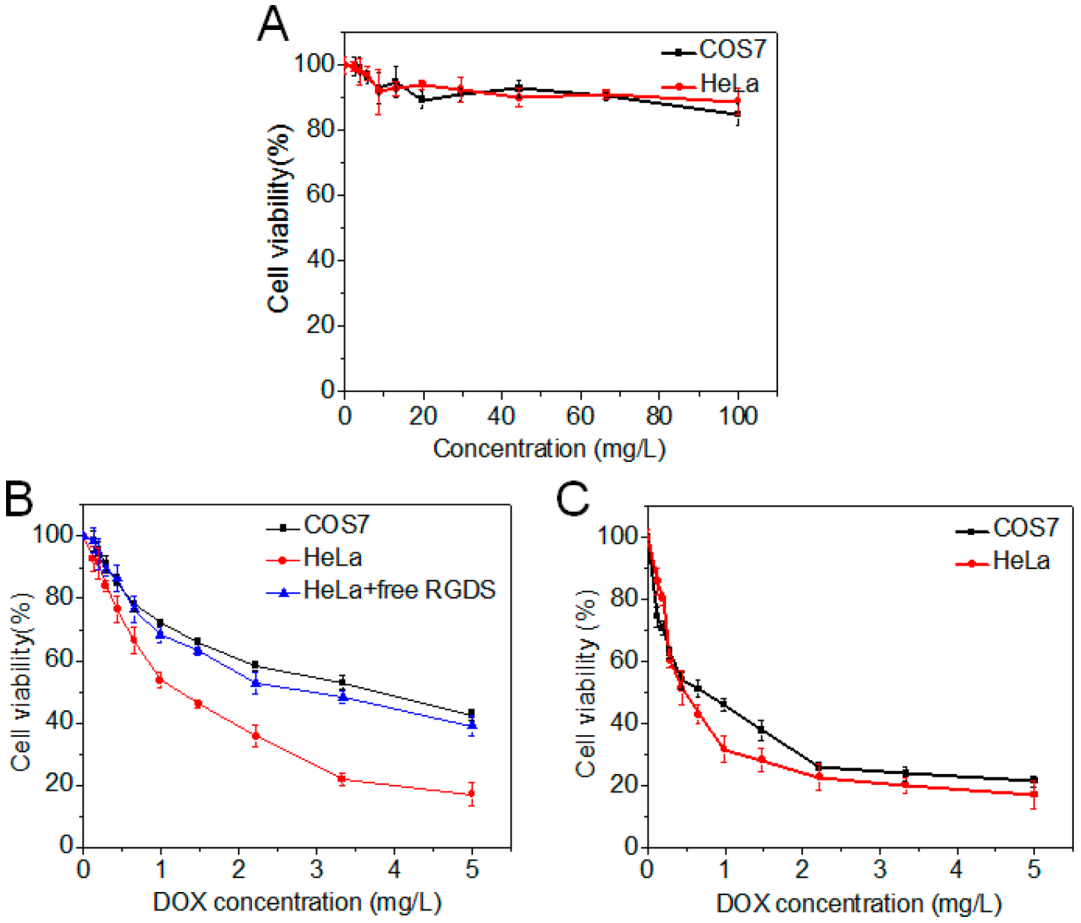


**Figure 7.** Viability of COS7 and HeLa cells incubated with blank MSN-GFLGR$_7$RGDS/$\alpha$-CD (A), DOX@MSN-GFLGR$_7$RGDS/$\alpha$-CD in the absence/presence of free RGDS peptide (2 $\mu$M) (B), and free DOX (C) for 48 h.

**Table 2. $IC_{50}$ Values of Free DOX and DOX@MSN-GFLGR$_7$RGDS/$\alpha$-CD Nanoparticles in HeLa and COS7 Cells**

| | DOX-loaded MSNs ($\mu$g/mL) | DOX-loaded MSNs + free RGDS ($\mu$g/mL) | free DOX ($\mu$g/mL) |
|---|---|---|---|
| HeLa | 1.2 | 4.3 | 0.49 |
| COS7 | 3.8 | | 0.74 |

~fourfold increase in the $IC_{50}$ (~4.3 $\mu$g/mL). In comparison with the free DOX (~0.49 $\mu$g/mL for HeLa cells and ~0.74 $\mu$g/mL for COS7 cells), there was an increase in the $IC_{50}$ of the DOX@MSN-GFLGR$_7$RGDS/$\alpha$-CD nanoparticles, but the selectivity was significantly improved, which was extremely important for clinical cancer chemotherapy.

## 4. CONCLUSIONS

In this study, a tumor-targeted and enzyme-induced drug-delivery system was designed and constructed by immobilizing cleavable rotaxanes onto MSNs. Instead of traditional host–guest interaction between cyclodextrin and adamantine, a multifunctional peptide azido-GFLGR$_7$RGDS was used to act as the enzyme-cleavable stopper for the cyclodextrin rotaxane valve through click chemistry. DOX@MSN-GFLGR$_7$RGDS/$\alpha$-CD has been proved to be capable of efficient uptake by tumor cells via cell integrins receptor-mediated targeting, and is superb for specifically delivering DOX into tumor cells via enzymatic digestion of GFLG peptide. Moreover, free RGDS peptides could compete for the $\alpha_v\beta_3$ sites on the cell membrane and reduce the access of DOX-loaded DOX@MSN-GFLGR$_7$RGDS/$\alpha$-CD to $\alpha_v\beta_3$ overexpressed HeLa cells, further confirming that the internalization of the nanoparticles was achieved via receptor-mediated endocytosis. We believe that the multifunctional MSNs demonstrated here can be used as a versatile nanoplatform for targetedly delivering therapeutic drug for cancer therapy. Considering the large size of designed MSNs in this study, a drug delivery system based on smaller MSNs is being constructed at present for in vivo anticancer therapy in further study.

## ■ ASSOCIATED CONTENT

### Ⓢ Supporting Information

BET and BJH parameters of synthesized MSNs; MALDI-TOF and ESI-MS spectra of peptides; size distribution of MSNs; FT-IR spectra of MSNs. The Supporting Information is available free of charge on the ACS Publications website at DOI: 10.1021/acsami.5b00752.

## ■ AUTHOR INFORMATION

### Corresponding Author

*Phone: +86 27 6875 4061. Fax: +86 27 6875 4509. E-mail: hefeng@whu.edu.cn.

### Author Contributions

All authors have given approval to the final version of the manuscript.



DOI: 10.1021/acsami.5b00752
ACS Appl. Mater. Interfaces 2015, 7, 9078–9087

### Notes

The authors declare no competing financial interest.

## ■ ACKNOWLEDGMENTS

We are grateful for the financial support of Natural Science Foundation of Hubei Province of China (Nos. 2014CFB696 and 2013CFA003), National Natural Science Foundation of China (No. 21074098), and National Key Basic Research Program of China (No. 2011CB606202).

## ■ ABBREVIATIONS

DOX, doxorubicin
MSNs, mesoporous silica nanoparticles
α-CD, α-cyclodextrin
nano-DDS, nanodrug delivery system
GFLG, Gly-Phe-Leu-Gly
RGDS, Arg-Gly-Asp-Ser
$R_7$, seven arginine
CTAB, *N*-cetyltrimethylammonium bromide
NaOH, sodium hydroxide
TEOS, tetraethylorthosilicate
$CuSO_4 \cdot 5H_2O$, copper(II) sulfate pentahydrate
NaAsc, sodium ascorbate
EDTA, ethylene diamine tetraacetic acid
TEA, triethylamine
TFA, trifluoroacetic acid
DMF, *N*,*N*-dimethylformamide
FMOC, *N*-fluorenyl-9-methoxycarbonyl
DiEA, diisopropylethylamine
HBTU, *o*-benzotriazol-*N*,*N*,*N*′,*N*′-tetramethyluronium hexafluorophosphate
HOBt, *N*-hydroxybenzotriazole
AAPTMS, γ-(2-aminoethyl)-aminopropyl trimethoxysilane
Hela, cervical cancer cells
COS 7, african green monkey SV40-transformed kidney fibroblast cells
DMEM, Dulbecco's Modified Eagle's Medium
PBS, phosphate buffered saline
FBS, fetal bovine serum
MTT, 3-(4,5-dimethylthiazol-2-yl)-2,5-diphenyltetrazolium bromide
HEPES (4-(2-hydroxyethyl)-1-piperazineethanesulfonic acid)
BCA, bicinchonininc acid
SDS-PAGE, polyacrylamide gelelectrophoresis
TBST, Tris-buffered saline-Tween 20
GAPDH, (glyceraldehyde-3-phosphate dehydrogenase)
SPPS, solid phase peptide synthesis
MALDI-TOF MS, matrix-assisted laser desorption/ionization time of flight mass spectrometry
ESI-MS, electrospray ionization-mass spectrometry
PDI, polydispersity index
$IC_{50}$, half-inhibitory concentration

## ■ REFERENCES

(1) Cho, K.; Wang, X.; Nie, S.; Shin, D. M. Therapeutic Nanoparticles for Drug Delivery in Cancer. *Clin. Cancer Res.* **2008**, *14*, 1310−1316.
(2) Sinha, A.; Chakraborty, A.; Jana, N. R. Dextran-Gated, Multifunctional Mesoporous Nanoparticle for Glucose-Responsive and Targeted Drug Delivery. *ACS Appl. Mater. Interfaces* **2014**, *6*, 22183−22191.
(3) Petros, R. A.; DeSimone, J. M. Strategies in the Design of Nanoparticles for Therapeutic Applications. *Nat. Rev. Drug Discovery* **2010**, *9*, 615−627.
(4) Slowing, I. I.; Vivero-Escoto, J. L.; Wu, C. W.; Lin, V. S. Y. Mesoporous Silica Nanoparticles as Controlled Release Drug Delivery and Gene Transfection Carriers. *Adv. Drug Delivery Rev.* **2008**, *60*, 1278−1288.
(5) Vivero-Escoto, J. L.; Slowing, I. I.; Trewyn, B. G.; Lin, V. S. Y. Mesoporous Silica Nanoparticles for Intracellular Controlled Drug Delivery. *Small* **2010**, *6*, 1952−1967.
(6) Tang, F.; Li, L.; Chen, D. Mesoporous Silica Nanoparticles: Synthesis, Biocompatibility and Drug Delivery. *Adv. Mater.* **2012**, *24*, 1504−1534.
(7) Meng, H.; Xue, M.; Xia, T.; Zhao, Y. L.; Tamanoi, F.; Stoddart, J. F.; Zink, J. I.; Nel, A. E. Autonomous In Vitro Anticancer Drug Release from Mesoporous Silica Nanoparticles by pH-Sensitive Nanovalves. *J. Am. Chem. Soc.* **2010**, *132*, 12690−12697.
(8) Li, Z.; Barnes, J. C.; Bosoy, A.; Stoddart, J. F.; Zink, J. I. Mesoporous Silica Nanoparticles in Biomedical Applications. *Chem. Soc. Rev.* **2012**, *41*, 2590−2605.
(9) Zhao, Y.; Trewyn, B. G.; Slowing, I. I.; Lin, V. S. Y. Mesoporous Silica Nanoparticle-Based Double Drug Delivery System for Glucose-Responsive Controlled Release of Insulin and Cyclic AMP. *J. Am. Chem. Soc.* **2009**, *131*, 8398−8400.
(10) Park, C.; Oh, K.; Lee, S. C.; Kim, C. Controlled Release of Guest Molecules from Mesoporous Silica Particles Based on a pH-Responsive Polypseudorotaxane Motif. *Angew. Chem., Int. Ed.* **2007**, *46*, 1455−1457.
(11) Zhao, Y. L.; Li, Z.; Kabehie, S.; Botros, Y. Y.; Stoddart, J. F.; Zink, J. I. pH-Operated Nanopistons on the Surfaces of Mesoporous Silica Nanoparticles. *J. Am. Chem. Soc.* **2010**, *132*, 13016−13025.
(12) Dong, L.; Peng, H.; Wang, S.; Zhang, Z.; Li, J.; Ai, F.; Zhao, Q.; Luo, M.; Xiong, H.; Chen, L. Thermally and Magnetically Dual-Responsive Mesoporous Silica Nanospheres: Preparation, Characterization, and Properties for the Controlled Release of Sophoridine. *J. Appl. Polym. Sci.* **2014**, DOI: 10.1002/APP.40477.
(13) Lee, J. E.; Lee, N.; Kim, H.; Kim, J.; Choi, S. H.; Kim, J. H.; Kim, T.; Song, I. C.; Park, S. P.; Moon, W. K.; Hyeon, T. Uniform Mesoporous Dye-Doped Silica Nanoparticles Decorated with Multiple Magnetite Nanocrystals for Simultaneous Enhanced Magnetic Resonance Imaging, Fluorescence Imaging, and Drug Delivery. *J. Am. Chem. Soc.* **2009**, *132*, 552−557.
(14) Vivero-Escoto, J. L.; Slowing, I. I.; Wu, C. W.; Lin, V. S. Y. Photoinduced Intracellular Controlled Release Drug Delivery in Human Cells by Gold-Capped Mesoporous Silica Nanosphere. *J. Am. Chem. Soc.* **2009**, *131*, 3462−3463.
(15) Zhang, R.; Li, L.; Feng, J.; Tong, L.; Wang, Q.; Tang, B. Versatile Triggered Release of Multiple Molecules from Cyclodextrin Modified Gold Gated Mesoporous Silica Nanocontainers. *ACS Appl. Mater. Interfaces* **2014**, *6*, 9932−9936.
(16) Zhao, J.; Lu, C.; He, X.; Zhang, X.; Zhang, W.; Zhang, X. Polyethyleneimine-Grafted Cellulose Nanofibril Aerogels as Versatile Vehicles for Drug Delivery. *ACS Appl. Mater. Interfaces* **2015**, *7*, 2607−2615.
(17) Tsai, C. P.; Chen, C. Y.; Hung, Y.; Chang, F. H.; Mou, C. Y. Monoclonal Antibody-Functionalized Mesoporous Silica Nanoparticles (MSN) for Selective Targeting Breast Cancer Cells. *J. Mater. Chem.* **2009**, *19*, 5737−5743.
(18) Trewyn, B. G.; Whitman, C. M.; Lin, V. S. Y. Morphological Control of Room-Temperature Ionic Liquid Templated Mesoporous Silica Nanoparticles for Controlled Release of Antibacterial Agents. *Nano Lett.* **2004**, *4*, 2139−2143.
(19) He, X.; Alves, C. S.; Oliveira, N.; Rodrigues, J.; Zhu, J.; Bányai, I.; Tomás, H.; Shi, X. RGD Peptide-Modified Multifunctional Dendrimer Platform for Drug Encapsulation and Targeted Inhibition of Cancer Cells. *Colloids Surf., B* **2015**, *125*, 82−89.
(20) Tian, Z.; Yang, C.; Wang, W.; Yuan, Z. Shieldable Tumor Targeting Based on pH Responsive Self-Assembly/Disassembly of


DOI: 10.1021/acsami.5b00752
*ACS Appl. Mater. Interfaces* 2015, 7, 9078−9087

Gold Nanoparticles. *ACS Appl. Mater. Interfaces* **2014**, *6*, 17865−17876.
(21) Zhang, J.; Yuan, Z. F.; Wang, Y.; Chen, W. H.; Luo, G. F.; Cheng, S. X.; Zhuo, R. X.; Zhang, X. Z. Multifunctional Envelope-Type Mesoporous Silica Nanoparticles for Tumor-Triggered Targeting Drug Delivery. *J. Am. Chem. Soc.* **2013**, *135*, 5068−5073.
(22) Gandavarapu, N. R.; Azagarsamy, M. A.; Anseth, K. S. Photo-Click Living Strategy for Controlled, Reversible Exchange of Biochemical Ligands. *Adv. Mater.* **2014**, *26*, 2521−2526.
(23) Popat, A.; Ross, B. P.; Liu, J.; Jambhrunkar, S.; Kleitz, F.; Qiao, S. Z. Enzyme-Responsive Controlled Release of Covalently Bound Prodrug from Functional Mesoporous Silica Nanospheres. *Angew. Chem., Int. Ed.* **2012**, *51*, 12486−12489.
(24) Foekens, J. A.; Kos, J.; Peters, H. A.; Krasovec, M.; Look, M. P.; Cimerman, N.; Meijer-Van Gelder, M. E.; Henzen-Logmans, S. C.; Van Putten, W. L.; Klijn, J. G. Prognostic Significance of Cathepsins B and L in Primary Human Breast Cancer. *J. Clin. Oncol.* **1998**, *16*, 1013−1021.
(25) Li, J.; Liu, F.; Shao, Q.; Min, Y.; Costa, M.; Yeow, E. K. L.; Xing, B. Enzyme-Responsive Cell-Penetrating Peptides Conjugated Mesoporous Silica Quantum Dots Nanocarriers for Controlled Release of Nucleus-Targeted Drug Molecules and Real-Time Intracellular Fluorescence Imaging of Tumor Cells. *Adv. Healthcare Mater.* **2014**, *3*, 1230−1239.
(26) Srinivasarao, M.; Galliford, C. V.; Low, P. S. Principles in the Design of Ligand-Targeted Cancer Therapeutics and Imaging Agents. *Nat. Rev. Drug Discovery* **2015**, *14*, 203−219.
(27) Patel, K.; Angelos, S.; Dichtel, W. R.; Coskun, A.; Yang, Y. W.; Zink, J. I.; Stoddart, J. F. Enzyme-Responsive Snap-Top Covered Silica Nanocontainers. *J. Am. Chem. Soc.* **2008**, *130*, 2382−2383.
(28) Foekens, J. A.; Kos, J.; Peters, H. A.; Krasovec, M.; Look, M. P.; Cimerman, N.; Meijer-Van Gelder, M. E.; Henzen-Logmans, S. C.; Van Putten, W. L.; Klijn, J. G. Prognostic Significance of Cathepsins B and L in Primary Human Breast Cancer. *J. Clin. Oncol.* **1998**, *16*, 1013−1021.
(29) Li, J.; Liu, F.; Shao, Q.; Min, Y.; Costa, M.; Yeow, E. K. L.; Xing, B. Enzyme-Responsive Cell-Penetrating Peptides Conjugated Mesoporous Silica Quantum Dots Nanocarriers for Controlled Release of Nucleus-Targeted Drug Molecules and Real-Time Intracellular Fluorescence Imaging of Tumor Cells. *Adv. Healthcare Mater.* **2014**, *3*, 1230−1239.
(30) Srinivasarao, M.; Galliford, C. V.; Low, P. S. Principles in the Design of Ligand-Targeted Cancer Therapeutics and Imaging Agents. *Nat. Rev. Drug Discovery* **2015**, *14*, 203−219.
(31) Zhang, C.; Wang, W.; Liu, T.; Wu, Y.; Guo, H.; Wang, P.; Tian, Q.; Wang, Y.; Yuan, Z. Doxorubicin-Loaded Glycyrrhetinic Acid-Modified Alginate Nanoparticles for Liver Tumor Chemotherapy. *Biomaterials* **2012**, *33*, 2187−2196.
(32) Guo, H.; Lai, Q.; Wang, W.; Wu, Y.; Zhang, C.; Liu, Y.; Yuan, Z. Functional Alginate Nanoparticles for Efficient Intracellular Release of Doxorubicin and Hepatoma Carcinoma Cell Targeting Therapy. *Int. J. Pharm.* **2013**, *451*, 1−11.
(33) Fields, G. B.; NOBLE, R. L. Solid Phase Peptide Synthesis Utilizing 9-Fluorenylmethoxycarbonyl Amino Acids. *Int. J. Pept. Protein Res.* **1990**, *35*, 161−214.
(34) Luo, G. F.; Chen, W. H.; Liu, Y.; Lei, Q.; Zhuo, R. X.; Zhang, X. Z. Multifunctional Enveloped Mesoporous Silica Nanoparticles for Subcellular Co-Delivery of Drug and Therapeutic Peptide. *Sci. Rep.* **2014**, *4*, 6064.
(35) Goel, S.; Chen, F.; Hong, H.; Valdovinos, H. F.; Hernandez, R.; Shi, R.; Barnhart, T. E.; Cai, W. $VEGF_{121}$-Conjugated Mesoporous Silica Nanoparticle: A Tumor Targeted Drug Delivery System. *ACS Appl. Mater. Interfaces* **2014**, *6*, 21677−21685.
(36) Yuan, Y.; Zhang, C. J.; Gao, M.; Zhang, R.; Tang, B. Z.; Liu, B. Specific Light-Up Bioprobe with Aggregation-Induced Emission and Activatable Photoactivity for the Targeted and Image-Guided Photodynamic Ablation of Cancer Cells. *Angew. Chem., Int. Ed.* **2015**, *54*, 1780−1786.
(37) Schmid, B.; Chung, D. E.; Warnecke, A.; Fichtner, I.; Kratz, F. Albumin-Binding Prodrugs of Camptothecin and Doxorubicin with an Ala-Leu-Ala-Leu-Linker That Are Cleaved by Cathepsin B: Synthesis and Antitumor Efficacy. *Bioconjugate Chem.* **2007**, *18*, 702−716.
(38) Qin, S. Y.; Xu, X. D.; Chen, C. S.; Chen, J. X.; Li, Z. Y.; Zhuo, R. X.; Zhang, X. Z. Supramolecular Architectures Self-assembled from Asymmetrical Hetero Cyclopeptides. *Macromol. Rapid Commun.* **2011**, *32*, 758−764.
(39) Yoo, H. S.; Lee, K. H.; Oh, J. E.; Park, T. G. In Vitro and In Vivo Anti-Tumor Activities of Nanoparticles Based on Doxorubicin-PLGA Conjugates. *J. Controlled Release* **2000**, *68*, 419−431.
(40) Zhang, Q.; Liu, F.; Nguyen, K. T.; Ma, X.; Wang, X.; Xing, B.; Zhao, Y. Multifunctional Mesoporous Silica Nanoparticles for Cancer Targeted and Controlled Drug Delivery. *Adv. Funct. Mater.* **2012**, *22*, 5144−5156.
(41) Zhang, C.; Pan, D.; Luo, K.; Li, N.; Guo, C.; Zheng, X.; Gu, Z. Dendrimer−Doxorubicin Conjugate as Enzyme-Sensitive and Polymeric Nanoscale Drug Delivery Vehicle for Ovarian Cancer Therapy. *Polym. Chem.* **2014**, *5*, 5227−5235.
(42) Rim, H. P.; Mi, K. H.; Lee, H. J.; Jeong, S. Y.; Lee, S. C. PH-Tunable Calcium Phosphate Covered Mesoporous Silica Nanocontainers for Intracellular Controlled Release of Guest Drugs. *Angew. Chem., Int. Ed.* **2011**, *50*, 8853−8857.


DOI: 10.1021/acsami.5b00752
*ACS Appl. Mater. Interfaces* 2015, 7, 9078−9087